

Localizing Retinotopic fMRI Activation in Human Primary Visual Cortex via Dynamic Programming

Anqi Qiu^{*†}, Benjamin J. Rosenau[‡], Adam S. Greenberg[‡], Patrick Barta^{*§¶},
Steven Yantis[‡] and Michael I. Miller^{*§}

^{*}Center for Imaging Science, Johns Hopkins University

[†]Department of Electrical and Computer Engineering, Johns Hopkins University

[‡]Department of Psychological and Brain Sciences, Johns Hopkins University

[§] Department of Biomedical Engineering, Johns Hopkins University

[¶] Department of Psychiatry, Johns Hopkins University School of Medicine

Abstract— This paper presents an approach for automatically delineating the borders of human primary visual cortex and finding ridges of maximal response due to static phase-encoding stimuli on fMRI *t*-statistical maps via dynamic programming. The sensitivity of such an approach to the choice of initial starting and ending points and the identification of the ridge path over a wide response region are addressed. Moreover, retinotopic maps for left and right visual cortex are shown in a population of two normal subjects.

I. INTRODUCTION

In 1918, Holmes [1] stated that the human primary visual cortex (V1) is retinotopically organized: adjacent neurons of the cortex correspond to adjacent locations in the visual field. Such retinotopic organization is described by eccentricity and polar angle mappings. The eccentricity mapping indicates that as a ring travels from the center to the periphery of the visual field, its representation in the visual cortex moves anteriorly from the occipital pole. Furthermore, the polar angle mapping implies that as one shifts from the upper vertical meridian through the horizontal to the lower vertical meridian in the visual field, the representation in the visual cortex moves superiorly from the lingual gyrus through the calcarine sulcus to the cuneus gyrus. However, the spatial sampling property, quantified by the linear cortical magnification factor [2] as the amount of cortex representing a unit degree of the visual field at a given eccentricity, was underestimated in the foveal region in early studies. Horton and Hoyt [3] in 1991 revised the Holmes map by using MRI. Since then, retinotopic organization in human V1 has been studied by using both static and traveling phase-encoding stimuli in fMRI studies [4]–[9]. However, automatic methods to define the functional borders of V1 and determine the correspondence between visual stimuli and fMRI statistical maps are still missing. Such methods are critical for estimating the linear cortical magnification in human primary visual cortex and they would open new clinical possibilities for the study of pathologic vision and inform the development of new strategies for rehabilitation [10]–[13].

This paper presents a procedure to delineate the borders of V1 from fMRI response to meridian stimuli and the ridges of

maximal activation due to eccentricity mapping stimuli via dynamic programming (DP) on the cortical surface. Subjects view seven annular rings of equal thickness that tile the visual field from 1.62 to 12.96 degrees of eccentricity, as well as vertical and horizontal meridia. Functional *t*-statistical maps are superimposed on the local coordinate system constructed from the gray/white matter boundary of the occipital lobe. The ridge of maximum activation on the surface due to each ring or wedge is estimated via DP optimization over all possible paths on the cortical surface. The sequentially additive costs for the DP are constructed from the maximal *t*-statistic superimposed on the local coordinate system.

II. METHODS

A. Preprocessing

For completeness, we briefly describe the procedure for functional and anatomical MRI analysis.

1) fMRI Experimental Design and Analysis.

Phase-encoded stimuli are used in this study. The V1-localizer consists of two wedges, each subtending 60 degrees of polar angle. The eccentricity mapping stimulus consists of seven annular rings of equal thickness that tile the visual field from 1.62 to 12.96 degrees of eccentricity. All stimuli are composed of 8Hz contrast reversing radial checkerboards with a central fixation disk.

Functional time series volumes are preprocessed using BrainVoyager 2000. Preprocessing steps include: slice acquisition time correction, within-run motion correction, temporal high-pass filtering, and temporal low-pass filtering. Because a bite bar ensures between-runs head stability, we use only within-runs motion correction to correct for transient motion as a result of bite bar disengagement. All analysis is performed within-subjects. For each subject, all runs of each type are normalized to a common mean and variance of scanner signal and concatenated. Stimulation and fixation blocks are modeled by boxcar functions convoluted with a canonical hemodynamic response function. For each run type, contrasts between relevant stimulus

types (V1-localizer: horizontal meridian vs. vertical meridian; eccentricity stimulus: each ring individually vs. fixation) are used to generate unthresholded t -statistical maps.

2) Anatomical MRI Analysis.

We first define the region of interest encompassing the occipital lobe in the anatomical MRI volume. Then, a Bayesian segmentation using the expectation-maximization algorithm to fit the compartmental statistics is used to label voxels as gray matter (GM), white matter (WM), and cerebrospinal fluid (CSF) in the subvolume [14], [15]. Surfaces are generated at the GM/WM interface by the topology-correction method [16], [17]. For visualization purposes, the cortical surface is bijectively mapped into the 2D-plane via the conformal mapping algorithm [18].

3) Surface-based Representation of Functional Response.

Functional t -statistical data in the gray matter region are assigned to the cortical surface weighted by the distance from the gray matter voxel to the cortical surface in the normal direction.

4) Smoothing Functional Maps on the Cortical Surface.

Surface-based representations of the functional responses due to each ring and the meridian stimulus are smoothed by using basis functions of the Laplace-Beltrami operator incorporating the geometry of the cortical surface with Neumann boundary conditions [19].

B. Ridge of Maximal Activation via DP

We localize the functional response to each annular ring stimulus on the smoothed functional map and build the correspondence between functional responses and annular rings in the visual field via DP. Because the blood oxygen level dependent (BOLD) fMRI response is an indirect and blurry measurement of the neural response, it is difficult to localize and separate the functional responses to each individual ring. Additionally, the location of a ring's response cannot be characterized by the boundaries of the activation, as these boundaries are threshold dependent. However, the location where the maximal activation to each ring occurs is independent of threshold and more reliable. Therefore, we use the ridge of the maximal activation to represent the ring's center on the cortical surface to avoid thresholding step. Such a ridge is defined as the path that has the minimal cost among candidate curves $\alpha(s, t)$ on the surface, where s and t are starting and ending points, respectively. The cost function is described as the form:

$$\int_{\alpha(s,t)} (r(\mathbf{x}) - R)^2 d\alpha, \quad (1)$$

where $r(\mathbf{x})$ is the functional statistic at the position \mathbf{x} on the surface. We use the t -statistic to characterize the functional response. R is assigned as the largest value of t -statistic on the surface.

DP is adapted to the above optimization problem on the triangulated surface [20]. Define N_v and N_T as the number of vertices and triangles on the surface \mathcal{M} , respectively. Denote the index of each vertex on the surface as $i, i = 1, 2, \dots, N_v$, and its coordinates in \mathbb{R}^3 as \mathbf{x}_i , and a triangle on the surface as $T_j, j = 1, 2, \dots, N_T$. If the vertex i is one of three vertices within triangle T_j , then we say $i \in T_j$. Define the platelet \mathcal{N}_i as the set of vertices, for which there is an edge e_{ij} connecting it with vertex i , written as

$$\mathcal{N}_i = \{j | e_{ij} \in \mathcal{M}, j = 1, 2, \dots, N_v, j \neq i\}.$$

Define a path on the surface routed and terminated respectively in vertices s and t on the surface as

$$(s = j_1, j_2), \dots, (j_{k-1}, j_k), \dots, (j_{N-1}, t = j_N),$$

such that $j_k \in \mathcal{N}_{j_{k-1}}$ for $\forall k$. Define the set of paths with connecting vertices s and t on the surface \mathcal{M} as $P(s, t)$, and $\alpha(s, t)$ as a path that belongs to $P(s, t)$. Then the ridge of maximal activation is defined as the cost-minimizing path given by

$$\hat{\alpha}(s, t) = \operatorname{argmin}_{\alpha(s,t) \in P(s,t)} \mathcal{C}_\alpha(s, t), \quad (2)$$

where

$$\mathcal{C}_\alpha(s, t) = \sum_{k=1}^N \left(R - \frac{r_{j_k} + r_{j_{k+1}}}{2} \right)^2 \| \mathbf{x}_{j_k} - \mathbf{x}_{j_{k+1}} \|. \quad (3)$$

Notice, when r is constant, $\hat{\alpha}$ is the path between vertices s and t with the shortest geodesic length on the surface. In addition, if the t -value is used, the ridge of minimal activation is defined in the same way by replacing R with the smallest t -value.

III. RESULTS

We show how to track the ridge of maximal activation, quantify the effect of the choice of starting and ending points on the surface, and illustrate how the ridge passes through the activation region. All ridge tracking results are visualized on the planar map, but all measurements are performed on the convoluted cortical surface.

A. Ridge Tracking

We first delimit the borders of V1 by defining the inferior and superior meridian ridges and mark the center of V1 by using the horizontal meridian response on the surface. Panels (a)-(c) in Fig. 1 show the functional map to the meridian wedges. Negative t -values denote the vertical meridian wedges (dark color) and positive t -values are associated with the horizontal meridian wedge (bright color). For ridges corresponding to the vertical meridian wedges, we manually initialize the starting and ending points, then the path, defined in Eq. 3 where R is the minimum t -value on the surface, is found via DP. The ridge for the horizontal meridian wedge is found in a similar way, except R is the maximum t -value on the surface in Eq. 3. We use the inferior and superior vertical meridian ridges on the surface as borders of V1. The horizontal meridian ridge separates V1 into two regions with which the lower and upper visual fields are associated. For ridge tracking of activations due to the ring

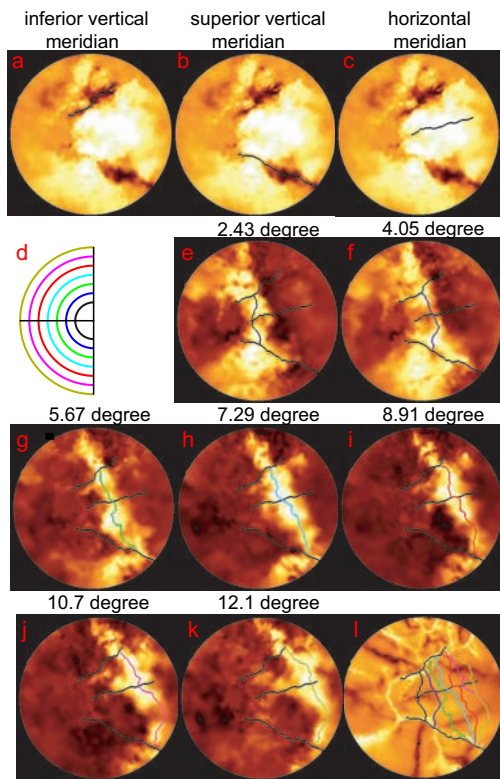


Fig. 1. Ridge tracking on the left occipital cortex. Panels (a)-(c) show vertical and horizontal meridians on the horizontal meridian map. Ridges of maximal activation are tracked by DP and are denoted by black lines. Panel (d) illustrates the left visual field with seven equal width rings. Each semi-circle represents the center of the ring indicated by different colors to be associated with the ridge tracked on functional maps shown on panels (e)-(k). Functional responses to each individual ring from 1.62 degrees to 12.96 degrees are shown on panels (e)-(k), respectively. The lines on these panels indicate the location of ridges of maximal activation associated with the center of each ring stimulus. The tops of panels give the eccentricity where the center of each ring stimulus is in the visual field. Brightness indicates the t value. Panel (l) gives the overall view of seven ridges on the 2D plane and the background shows the curvature information (bright: gyrus; dark: sulcus).

stimuli shown on panels (e)-(k), all starting and ending points reside on the inferior and superior vertical meridian ridges defined on panels (a)-(b). Panel (d) shows the center of each ring in a different color in the visual field and panels (e)-(k) illustrate the ridges of maximal activation to each ring on the surface, using the same color scheme. As visual field eccentricity increases, the functional ridges move from posterior to anterior occipital cortex as summarized on panel (l). The background of panel (l) gives the cortical surface curvature information, which is different from other panels (functional responses).

B. Convergence of Tracks

The tracking procedure described previously involves the manual selection of the starting and ending points for DP. Fig. 2 illustrates the effect of those initial points. Panels (a) and (b) show the functional map (shown on panel (e) of Fig. 1 as well) on the surface and plane, respectively. Red, blue, and green paths are tracks with different initial points separated

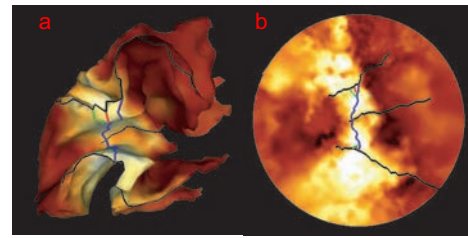


Fig. 2. Sensitivity analysis of DP for variation of starting and ending points in ridge tracking. Panels (a)-(b) show the functional map on the surface and plane, respectively. Three paths in red, blue, and green are tracked by giving different starting and ending points to find the ridge of maximal activation.

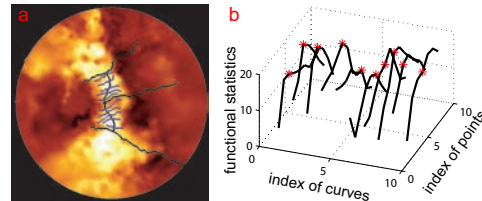


Fig. 3. Definiteness of ridge tracking. Panel (a) gives the functional map to the first ring that is also shown in Fig. 2(b). Ten blue curves are randomly defined so that they cross the ridge of maximal activation due to the first ring. They are indexed as $1, 2, \dots, 10$ from the top to the bottom. Panel (b) demonstrates the functional statistic of the ridge in the activation region. The x-axis indexes blue curves; the y-axis indexes the points on each blue curve; the z-axis shows the functional statistic for each point of the curve. Red *s represent the points where the ridge goes through.

by about 2 mm. These three paths converge between the inferior and superior meridian ridges after only two or three tracking nodes.

C. Definiteness

Fig. 3 illustrates the distribution of functional t -statistics in the direction parallel to the horizontal meridian and tests the ridge path through the wide swatch of fMRI activation due to a single eccentricity mapping ring. We randomly define ten curves roughly parallel to the horizontal meridian ridge (approximately perpendicular to the ridge due to the ring), colored blue on panel (a). These curves are indexed as $1, 2, \dots, 10$ from the top to the bottom. The points on the curves are also indexed as $1, 2, \dots, M$. The value of the functional statistic as a function of these indices is illustrated on panel (b), where x, y, z axes are index of curves, index of points on the curves, and functional statistic, respectively. Red *s give locations where the ridge passes. The ridge clearly crosses each curve roughly at the point where the maximum functional t -statistic occurs without taking the distance effect into account.

D. Retinotopic Eccentricity Map

Fig. 4 shows retinotopic eccentricity maps of human primary visual cortex in a population of two normal subjects. Panels (b)-(c) show such maps for the left and right visual cortical surfaces, on which each ridge is colored as its associated ring in the visual field on panel (a). The left occipital cortex is stimulated by the right visual field, while

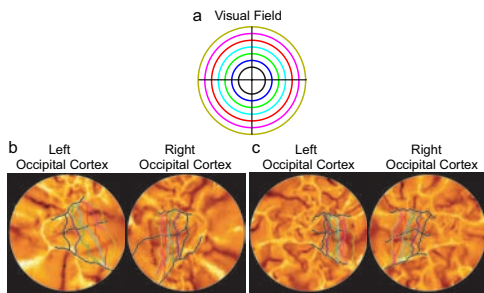


Fig. 4. Retinotopic Eccentricity Maps. Panel (a) gives a schematic denoting the centers of seven rings in the visual space, each a different color. The remaining panels illustrate the ridges of responses on the left and right visual cortical surfaces for each subject, respectively. Brightness indicates the curvature information.

the right occipital cortex is activated by the left visual field.

IV. DISCUSSION

Many optimization problems can be described as seeking the minimum (or maximum) cost path through a graph where the cost of a path is given by sequentially additive costs in the path. In such problems DP leads to a computationally efficient identification of the globally optimal path. Such an approach has been used in speech and character recognition, soft decoding, and road tracking. The interactive segmentation and automatic region of interest tracking in medical images via DP was proposed [21] in 1995. Also, Khaneja et. al. [20] delineated the principal curves (gyrus or sulcus) on the cortical surface generated from an anatomical MRI volume in 1998, followed by the study of extracting brain subcortical regions defined by the principal curves as anatomical landmarks [22].

In this paper, the dynamic programming approach identifies the global optimal path for the optimization procedure seeking the best curve associated with the maximal activation on the triangulated cortical surface. DP makes it possible to define the borders of V1 and build the correspondence between locations of the visual field and responses on the visual cortex in eccentricity mapping studies. This approach will help further understanding of the spatial sampling property of human primary visual cortex. The quantitative measurement of the spatial sampling property, the linear cortical magnification factor, can be directly computed on the cortical surface as the ratio of geodesic distance between the ridges to the eccentricity difference between the stimulus rings. Estimates of linear cortical magnification based on areas of intact vision in individuals with partially lesioned retinas will allow the quantitative investigation of cortical plasticity in human visual cortex.

ACKNOWLEDGEMENTS

The authors would like to thank Dr. Monica Hurdal of Florida State University for the bijective mapping. The work reported here was supported by NIH grant: R01-EB00975.

REFERENCES

- [1] G. Holmes, "Disturbances of vision by cerebral lesions," *Br J Ophthalmol*, vol. 2, p. 353C384, 1918.
- [2] P. Daniel and D. Whitteridge, "The representation of the visual field on the cerebral cortex in monkeys," *J Physiol*, vol. 159, pp. 203–221, 1961.
- [3] J. C. Horton and W. F. Hoyt, "The representation of the visual field in human striate cortex. a revision of the classic Holmes map," *Arch Ophthalmol*, vol. 109, pp. 816–824, 1991.
- [4] S. A. Engel, D. E. Rumelhart, B. A. Wandell, A. T. Lee, G. H. Glover, E. J. Chichilnisky, and M. N. Shadlen, "fMRI of human visual cortex," *Nature*, vol. 369, p. 525, 1994.
- [5] M. Sereno, A. M. Dale, J. B. Reppas, K. K. Kwong, J. W. Belliveau, B. T. J., B. R. Rosen, and R. B. Tootell, "Borders of multiple visual areas in humans revealed by functional magnetic resonance imaging," *Science*, vol. 268, pp. 889–893, 1995.
- [6] S. A. Engel, G. H. Glover, and B. A. Wandell, "Retinotopic organization in human visual cortex and the spatial precision of functional MRI," *Cerebral Cortex*, vol. 7, pp. 181–192, 1997.
- [7] R. B. H. Tootell, J. D. Mendola, N. K. Hadjikhani, P. J. Ledden, A. K. Liu, J. B. Reppas, M. I. Sereno, and A. M. Dale, "Functional analysis of V3A and related areas in human visual cortex," *J. Neurosci.*, vol. 17, pp. 7060–7078, 1997.
- [8] E. A. DeYoe, G. J. Carmandagger, P. BandettiniDagger, S. Glickman, J. Wieser, R. Cox, D. Miller, and J. Neitz, "Mapping striate and extrastriate visual areas in human cerebral cortex," *Proc. Natl. Acad. Sci.*, vol. 93, pp. 2382–2386, 1996.
- [9] R. Duncan and G. Boynton, "Cortical magnification within human primary visual cortex correlates with acuity thresholds," *Neuron*, vol. 38, pp. 659–671, 2003.
- [10] H. A. Baseler, A. B. Morland, and B. A. Wandell, "Topographic organization of human visual areas in the absence of input from primary cortex," *J. Neurosci.*, vol. 19, pp. 2619–2627, 1999.
- [11] A. B. Morland, H. A. Baseler, M. B. Hoffmann, L. T. Sharpe, and B. A. Wandell, "Abnormal retinotopic representation in human visual cortex revealed by fMRI," *Acta Psychol*, vol. 107, pp. 229–247, 2001.
- [12] J. S. Sunness, T. Liu, and S. Yantis, "Retinotopic mapping of the visual cortex using functional magnetic resonance imaging in a patient with central scotomas from atrophic macular degeneration," *Ophthalmology*, vol. 111, pp. 1595–1598, 2004.
- [13] C. I. Baker, E. Peli, N. Knouf, and N. G. Kanwisher, "Reorganization of visual processing in macular degeneration," *J. Neurosci.*, vol. 25, pp. 614–618, 2005.
- [14] M. Joshi, J. Cui, K. Doolittle, S. Joshi, D. Van Essen, L. Wang, and M. I. Miller, "Brain segmentation and the generation of cortical surfaces," *NeuroImage*, vol. 9, pp. 461–476, 1999.
- [15] M. I. Miller, A. B. Massie, J. T. Ratnanather, K. N. Botteron, and J. G. Csermanskyy, "Bayesian construction of geometrically based cortical thickness metrics," *NeuroImage*, vol. 12, pp. 676–687, 2000.
- [16] X. Han, C. Xu, D. Tosun, and J. L. Prince, "Cortical surface reconstruction using a topology preserving geometric deformable model," in *Workshop on Mathematical Methods in Biomedical Image Analysis*, Kauai Hawaii, Dec 2001, pp. 213–220.
- [17] X. Han, C. Xu, U. Braga-Neto, and J. Prince, "Topology correction in brain cortex segmentation using a multiscale, graph-based algorithm," *IEEE Trans. Med. Imag.*, vol. 21, pp. 109–121, 2002.
- [18] M. K. Hurdal, P. L. Bowers, K. Stephenson, D. L. Sumners, K. Rehm, K. Schaper, and D. A. Rottenberg, "Quasi-conformally flat mapping the human cerebellum," in *Lecture Notes in Computer Science*, C. Taylor and A. Colchester, Eds. Berlin: Springer-Verlag, 1999, pp. 279–286.
- [19] A. Qiu, D. Bitouk, and M. I. Miller, "Smooth functional and structural maps on the neocortex via orthonormal bases of the Laplace-Beltrami operator," *submitted to IEEE transactions on medical imaging*, 2005.
- [20] N. Khaneja, M. I. Miller, and U. Grenander, "Dynamic programming generation of curves on brain surfaces," *IEEE Trans. Pattern Anal. Mach. Intell.*, vol. 20, pp. 1260–1265, 1998.
- [21] D. Geiger, A. Gupta, L. A. Costa, and J. Vlontzos, "Dynamic programming for detecting, tracking, and matching deformable contours," *IEEE Trans. Pattern Anal. Mach. Intell.*, vol. 17, pp. 294–302, 1995.
- [22] J. T. Ratnanather, P. E. Barta, H. N. A., N. Lee, N. G. Morris, A. C. Dziorny, M. K. Hurdal, G. D. Pearlson, and M. I. Miller, "Dynamic programming generation of boundaries of local coordinatized sub-manifolds in the neocortex: application to the planum temporale," *NeuroImage*, vol. 20, no. 1, pp. 359–377, 2003.